

Torsional deformation and rotary driving characteristics of SMA thin strip

H. TOBUSHI¹⁾, E. A. PIECZYSKA²⁾, W. K. NOWACKI²⁾,
T. SAKURAGI³⁾, Y. SUGIMOTO¹⁾

¹⁾*Department of Mechanical Engineering
Aichi Institute of Technology
1247, Yachigusa, Yakusa-cho, Toyota, 470-0392, Japan
e-mail: tobushi@aitech.ac.jp*

²⁾*Institute of Fundamental Technological Research
Polish Academy of Sciences
Pawińskiego 5b, 02-106 Warsaw, Poland*

³⁾*Aikoku Alpha Co.
Hongou 11, Morikami, Sobue-cho, Inazawa, Aichi 495-8501, Japan*

THE TORSIONAL DEFORMATION PROPERTIES of a TiNi shape-memory alloy thin strip were investigated. The results obtained are summarized as follows. (1) The martensitic transformation starts at the edge of the thin strip. (2) The torsional deformation properties change slightly under thermomechanical cycling. (3) The fatigue life in pulsating torsion is longer than that in alternating torsion. (4) A simple rotary driving element can be developed by using the SMA thin strip.

Key words: shape memory alloy, thin strip, torsion, cyclic deformation, fatigue, rotary driving element.

Copyright © 2009 by IPPT PAN

1. Introduction

IN RECENT YEARS, the intelligent materials having the functions of sensing, judging and working, have attracted worldwide attention. One of the main materials which have activated the research on the intelligent materials is shape memory alloy (SMA) [1–5]. The main characteristics of SMA are the shape memory effect (SME) and superelasticity (SE). Thanks to these characteristics, SMAs are used in the driving elements of actuators, heat engines and robots. In the SMAs used in practical applications, TiNi SMAs are the most widely employed, since their grain size is small and there is little risk of inducing fatigue damage; in other words, they have a high fatigue strength and a long fatigue life [6–8]. The SME and SE appear as a result of a martensitic transformation (MT).

The deformation properties of the SME and SE depend strongly on temperature and stress. Because of the adaptable thermal response of SMA elements, thin wires and thin tapes are widely used in practical applications. These materials are on the market and can be obtained easily. The main loading conditions in these applications tend to be tension, compression, bending and torsion. In a recent study using the torsional deformation of a TiNi SMA tube, twist in the blades of rotor aircraft was investigated in order to improve the flight performance [9, 10].

In practical applications, making use of SMA thin strips, torsional deformation can be obtained simply by gripping both ends without any mechanical process. If the characteristics of SE are exploited, a high performance of energy storage can be achieved similar to that of a torsion bar. In this way of using torsional characteristics of SMA thin strips, simple and small actuators can be developed. In the case of an SMA thin strip twisted by fixing both ends which may be employed in practical applications, not only torsional but also tensile stress can be induced along both edges of the strip. As the shearing deformation properties of the material and the thermomechanical properties under multi-axial stress states are not clear, the deformation properties of the SMA thin strip in torsion can not be precisely estimated by the deformation properties of SMA wires and tubes, which have been obtained till now. The authors investigated therefore the basic deformation properties of an SMA thin strip in torsion [11].

In the present study, in order to develop the rotary driving elements of SMA thin strips, the tensile deformation properties along the edge of a TiNi SMA thin strip are investigated in torsion. The cyclic torsional deformation properties, which are important in the driving elements, are also investigated. The fatigue properties are investigated in pulsating torsion and alternating torsion. The two-way rotary movement of an opening and closing door driven by SMA thin strips is demonstrated.

2. Experimental method

2.1. Materials and specimen

The materials used in the experiment were Ti-50.18at%Ni SMA thin strip with a thickness of $t = 0.25$ mm and a width of $w = 5$ mm produced by Furukawa Electric Co., Ltd. The specimen was a uniform flat tape of length $L = 60$ mm. The gauge length of the specimen was $l = 40$ mm and the length held in the gripping device was 10 mm at each end. The as-received material was heat-treated in an electric furnace to memorize the flat plane. In this heat-treatment, the as-received material was first fixed in a flat plane, heated up

to 673 K for 2 hours and kept at 673 K for 1 hour, followed by cooling in the furnace. The transformation temperatures obtained from the differential scanning calorimetry (DSC) test were $M_s = 304$ K, $M_f = 266$ K, $A_s = 319$ K and $A_f = 359$ K.

2.2. Experimental apparatus

In order to perform the torsion test and torsion fatigue test, the following two experimental apparatuses were used.

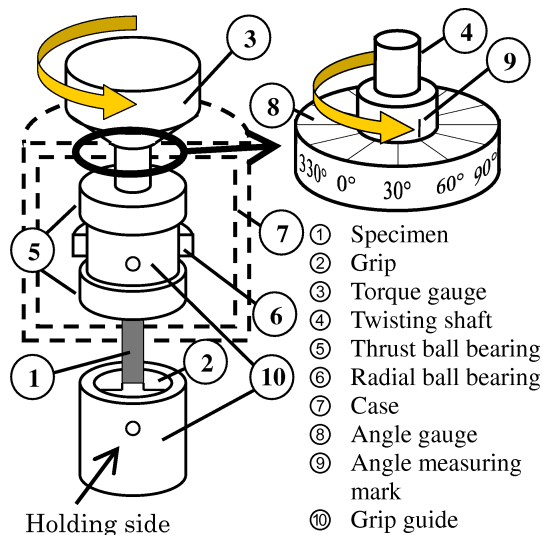


FIG. 1. Experimental apparatus for torsion test.

(1) Experimental apparatus for torsion test

A schematic drawing of the experimental apparatus for the torsion test is shown in Fig. 1. A specimen ① is held by the two grips ② in the experimental apparatus. The grip consists of two half-round bars with a groove. The specimen instead of groove, sandwiched between the half-round bars and pressed by a screw. The upper side of the grip ② and a torque gauge ③ are connected with a twisting shaft ④. By twisting the torque gauge, the specimen is therefore twisted and the torque is measured. By considering the mechanism of the practical rotary driving elements, a thrust ball bearing ⑤ is used in order to held the axial position constant through a grip guide ⑩. A radial ball bearing ⑥ is used in order to keep the center axial symmetry of the twisting shaft constant. The angle of twist is measured by using an angle measuring mark ⑨ attached to the twisting shaft and an angle gauge ⑧ fixed on the top of the case ⑦. In the case of cyclic torsion in air, the specimen was heated under no-load after unloading. The heating was

performed by passing a conducting wire through a small transverse hole provided in the grip ②, by winding the end of the conducting wire on a bolt touched to a specimen-fixing jig, and by using Joule heat through electric current. The tests were carried out in water except for the test at room temperature (RT) in air. The water temperature was controlled by using a temperature controller and a thermocouple. The temperature of the specimen was assumed to be equal to that of water.

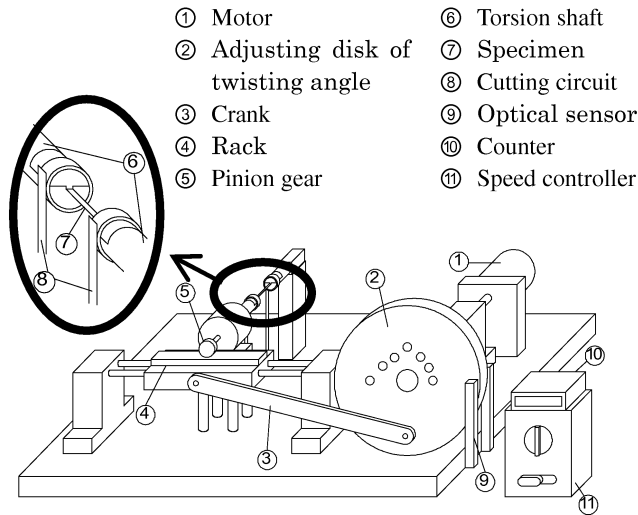


FIG. 2. Experimental apparatus for torsion fatigue test.

(2) Experimental apparatus for torsion fatigue test

A schematic drawing of the experimental apparatus for the torsion fatigue test is shown in Fig. 2. Rotary movement is transmitted from a motor ① to the adjusting disk for the angle of twist ② and then converted into reciprocating motion by means of a crank ③. By means of rack ④ and a pinion gear ⑤, the reciprocating motion is then reconverted into rotational motion. The angle of twist is controlled by changing the amount of movement of the rack through the adjusting disk of twisting angle. By fixing the specimen ⑦ on a torsion shaft ⑥ connected with the pinion gear, the specimen can be twisted repeatedly.

The specimen is twisted by the driving end of the torsion shaft connected with the pinion gear. In order to meet the condition that no axial displacement should appear during twisting, both ends are fixed on the line of the center axis. The number of cycles is measured using an optical sensor ⑨ and a counter ⑩. The rotational speed is controlled by a speed controller ⑪. By using the cutting circuit ⑧, the motor stops automatically when the specimen fails.

2.3. Experimental procedure

The torsion test and the torsion fatigue test were carried out as follows.

(1) Torsion test

The specimen was first held by the grips and the grips were fixed on the twisting shaft. The specimen was twisted at the prescribed angle of twist per unit length θ (total angle of twist ϕ). The angle of twist and torque were measured simultaneously. In the torsion test, the maximum angle of twist per unit length was applied and torque was completely removed during unloading. In the case of temperature $T = \text{RT}$, the specimen was heated under no-load after unloading. In the case of cyclic torsion test, it was loaded again after unloading followed by heating, and these processes were repeated till 50 cycles. The variation in torque was measured for each angle of twist during the repeated loading and unloading processes. The test temperatures T were RT and 358 K. The test was carried out in air at $T = \text{RT}$ and in water at 358K. The interval for measuring the angle of twist per unit length $\Delta\theta$ was $4.4 \text{ rad} \cdot \text{m}^{-1}$ (interval for the total angle of twist $\Delta\phi = \pi/18$). The maximum angle of twist per unit length θ_{\max} was $78.5 \text{ rad} \cdot \text{m}^{-1}$ (maximum total angle of twist $\phi_{\max} = \pi$). In the torsion test at RT, the temperature distribution on the whole surface of the specimen was measured by the infrared thermography. Before the testing, the specimen surface was covered with a very thin layer of carbon black powder in order to make its emissivity higher and more homogeneous. It should be noticed that a correct temperature measurement requires that the angle between the normal of the surface and the axis of the camera should be less than 45° .

(2) Torsion fatigue test

The prescribed angle of twist was first set using an adjusting disk for the angle of twist. The specimen was fixed to the torsion shaft and twisted cyclically at room temperature in air at the amplitude of the prescribed angle of twist, and the number of cycles to failure was measured. The frequency was 600 cpm (10 Hz) and the maximum angle of twist per unit length θ_{\max} was $34.9 \sim 78.5 \text{ rad} \cdot \text{m}^{-1}$ (maximum total angle of twist $\phi_{\max} = 4\pi/9 \sim \pi$). The twisting angle ratio $R_\theta = \theta_{\min}/\theta_{\max}$ was -1 for the alternating torsion fatigue test and 0 for the pulsating torsion fatigue test, respectively. To be sure of attaining the fatigue limit, the maximum number of cycles was set above 10^6 cycles.

3. Experimental results and discussion

3.1. Tensile deformation properties

The stress-strain curves obtained from the tension test for the SMA thin strip at temperature $T = \text{RT}$ and 363 K are shown in Fig. 3. In the test, it

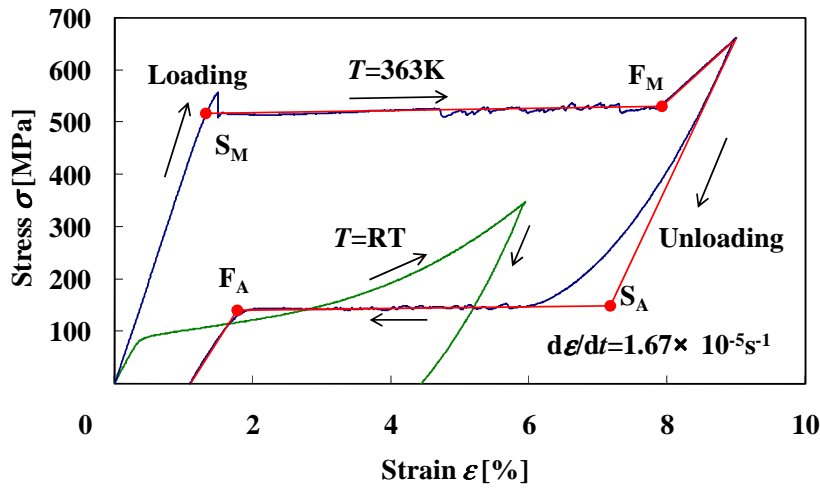


FIG. 3. Stress-strain curves in tension.

was loaded and unloaded under strain rate of $1.67 \times 10^{-5} \text{ s}^{-1}$. As can be seen in Fig. 3, an overshoot appears in the loading process in the vicinity of strain = 1% at $T = 363 \text{ K}$. An upper stress plateau appears from there on and finishes in the vicinity of strain = 7.5%. In the unloading process, the lower stress plateau starts in the vicinity of strain = 6% and ends at strain = 1.7%. The stress-strain curve draws a large hysteresis loop, showing the behavior of SE. Large strain variation due to the main MT and reverse transformation appears under the upper stress plateau in the loading process and the lower stress plateau in the unloading process, respectively. However, it should be noticed that the MT starts before the start point of the upper stress plateau S_M and still occurs after the finish point F_M , and the reverse transformation starts before the start point of the lower stress plateau S_A and still occurs after the finish point F_A [12–14].

At $T = \text{RT}$, the yielding phenomenon appears at strain of 0.3% and a residual strain of 4.5% appears after unloading. The residual strain disappears when heating occurs under no load, showing the SME.

3.2. Torsional deformation properties

In the present study, the thin strip was twisted from one end while both ends were held constant at the axial direction. The deformed state, the elongation of the edge of the strip and the temperature distribution on the surface of the strip were investigated.

(1) Deformation state

Photographs of the deformed SMA thin strip under torsion are shown in Fig. 4 for each angle of twist. In Fig. 4, the left side in each case shows the fixed end and the right side shows the twisted end.

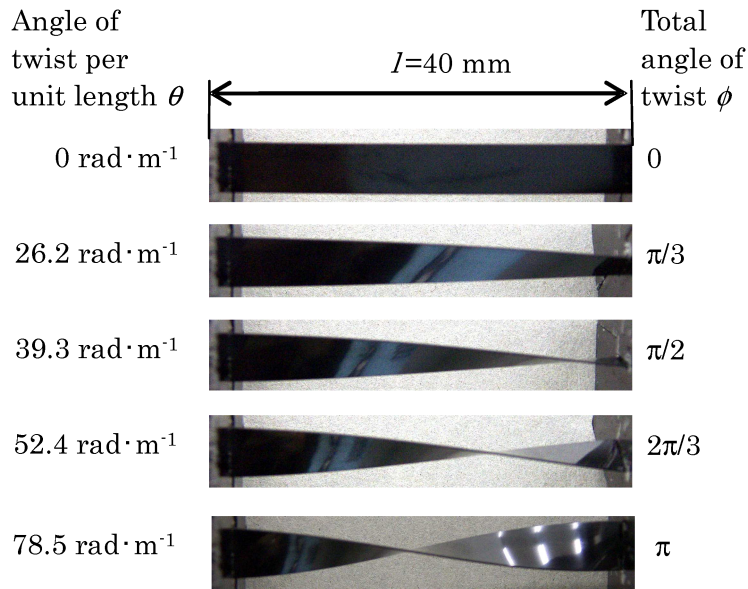


FIG. 4. Photographs of twisted SMA thin strip at each angle of twist.

As can be seen, the upper and lower surfaces of the SMA thin strip are reversed during twisting and a crossover point appears in the twisting end at the angle of twist per unit length $\theta = 39.3 \text{ rad} \cdot \text{m}^{-1}$ (total angle of twist $\phi = \pi/2$). The crossover point propagates from the twisting end and reaches the central part of the specimen at the angle of twist per unit length $\theta = 78.5 \text{ rad} \cdot \text{m}^{-1}$ (total angle of twist $\phi = \pi$). Comparing the initial state at $\theta = 0$ ($\phi = 0$) and the deformed state at $\theta = 78.5 \text{ rad} \cdot \text{m}^{-1}$ ($\phi = \pi$), both edges of the thin strip are elongated by twisting since both ends are axially fixed. Therefore, tensile stress is induced along both edges, and the stress state becomes different from the simple shear and much more complex.

(2) Elongation of edge in a thin strip

Elongation of the edge in the SMA thin strip was measured as follows. Two thin wires of length $l/2 = 20$ mm were pasted on the edge of SMA thin strip and the gap between two wires was measured by a thickness gauge. Tensile strain ε of the edge obtained from the torsion test at temperature $T = \text{RT}$ is shown in Fig. 5. As can be seen, tensile strain of the edge in the SMA thin strip increases in proportion to the increase in angle of twist per unit length, and the rate of increase in tensile strain grows gradually. In contrast, the calculated result obtained by assuming that the deformed state of the edge in the thin strip with a width w subjected to torsion is equal to a helix on the surface of a column with a diameter w , is shown by a dashed line in Fig. 5. As can be seen, the rate of increase in tensile strain of the helix $d\varepsilon/d\theta$ increases with an increase in angle

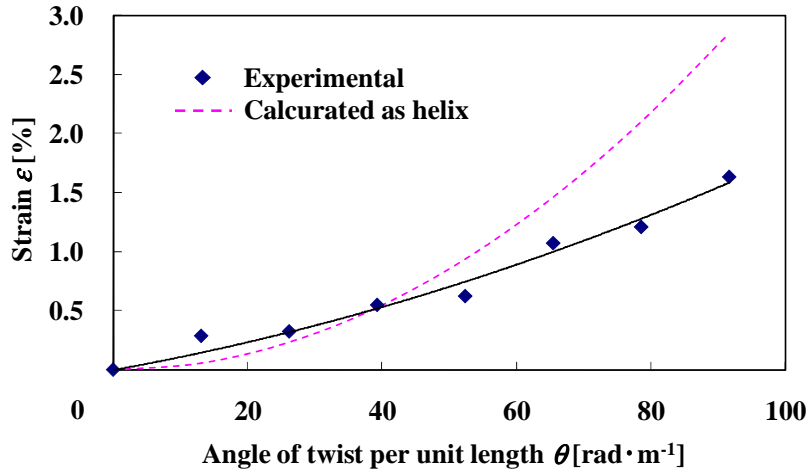


FIG. 5. Strain for the edge of the thin strip under torsion.

of twist per unit length θ . Comparing tensile strain of the experimental result and the calculated result, tensile strain of the edge in the strip appears from the initial stage of the deformation. Since the surface on the strip warps if angle of twist θ becomes large and the distance between the edges of the strip becomes therefore smaller than the helix on the column with a constant diameter, the rate of increase in actual tensile strain does not become so large, as shown by the solid line.

The angle of twist per unit length θ which corresponds to the MT starting strain of 0.3% at $T = \text{RT}$ is $25 \sim 30 \text{ rad} \cdot \text{m}^{-1}$. This angle of twist per unit length $\theta = 30 \text{ rad} \cdot \text{m}^{-1}$ for the MT starting strain is almost the same as the MT starting angle of twist per unit length, which was obtained in the previous paper [11] by assuming that the torsional MT stress τ_M satisfies the Mises yield condition [15], by determining $\tau_M = \sigma_M / \sqrt{3}$ from the tensile MT stress σ_M and by using the equation on torsional stress for thin strip in the theory of elasticity [16].

(3) Observation of deformation behavior by thermography

The thermomechanical characteristics of SMA appear due to the MT and the reverse transformation. The exothermic reaction and endothermic reaction occur based on the MT and the reverse transformation, respectively. In the DSC test, the transformation temperatures are determined by measuring the heat change owing to these reactions. In the case of SE due to the stress-induced MT, temperature increases and decreases in the loading and unloading processes, respectively. The initiation and growth processes of the MT can be therefore analyzed by measuring temperature on the surface of the material. The infrared thermography to measure the temperature distribution on the whole surface of

the material can be applied to this objective. The MT behavior of SMA can be analyzed by the thermography [14]. It should be noticed that the temperature fields depend not only on the heat sources but also on conduction and convection phenomena, and therefore depend on the torsion rate.

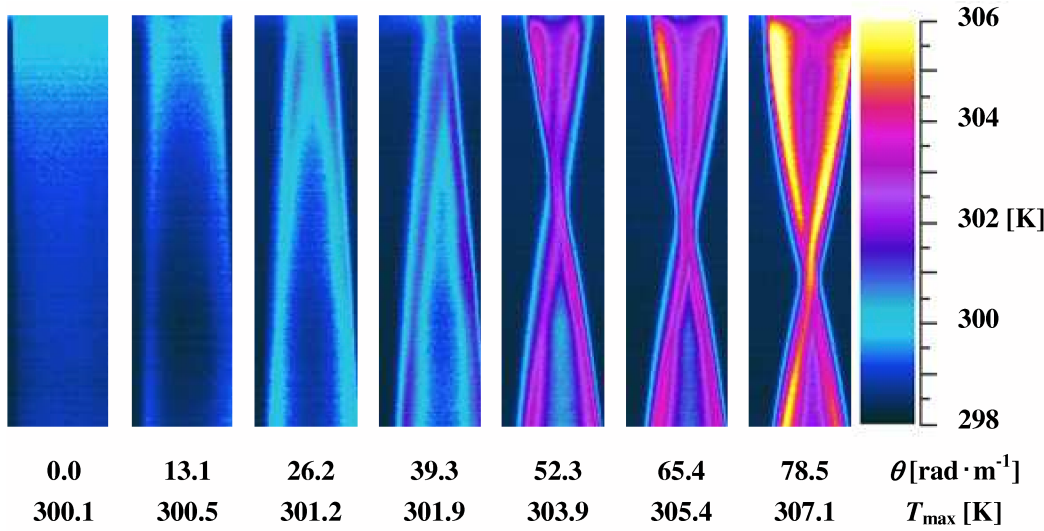


FIG. 6. Thermograms showing temperature distribution on the surface of the SMA thin strip due to the phase transformation under torsion.

The temperature distribution on the surface of the SMA thin strip at each angle of twist during the torsional deformation obtained by the infrared thermography is shown in Fig. 6. In Fig. 6, the upper side in each case shows the twisting part and the lower side shows the fixed part.

As can be seen in Fig. 6, maximum temperature T_{\max} on the surface of the specimen appears along the edge of the thin strip, and the exothermic MT occurs in this part and grows toward the central part of the specimen. The temperature rise along the edge of the strip starts at the angle of twist per unit length $\theta = 13.1 \text{ rad} \cdot \text{m}^{-1}$. At this twisting angle, the temperature field is not homogeneous and the temperature rise along the edge of the thin strip is 0.4 K. The temperature increases markedly at $\theta = 26.2 \text{ rad} \cdot \text{m}^{-1}$. This angle of twist per unit length corresponds to the tensile strain at the edge of the strip of 0.3% observed in Fig 5 and it shows that the MT occurs before the starting point S_M of the upper stress plateau. On the contrary, considering the stress distribution in the rectangular cross-section of the strip subjected to elastic deformation, it may be considered that the MT occurs at the central surface of a long side where torsional stress takes a maximum value [16]. However, as can be seen from Fig. 6, maximum temperature of the specimen occurs along the edge of the thin strip and the high temperature region propagates toward the central part with

an increase in angle of twist. Therefore, the MT grows preferentially based on the elongation along the edge of the strip, compared to the torsional strain at the central part of the strip. It is found therefore that the MT in the thin strip under torsion can not be analyzed by simple torsion.

With respect to the results on the temperature distribution obtained from the thermography shown in Fig. 6, the following points should be noticed. In the case of twisting the thin strip, the surface of the specimen is flat in the initial state without deformation, and is perpendicular to the axis of the camera to measure the temperature. The surface of the specimen becomes warped during twisting and inclined to the axis of the camera, and focus of the whole surface on the specimen varies. Although the temperature shown in Fig. 6 indicates the inclination of temperature distribution on the whole surface, temperature at each point does not indicate precise values. We should be therefore careful in evaluation of the temperature.

3.3. Cyclic torsion-deformation properties

The relations between torque M and angle of twist per unit length θ at the number of cycles $N = 1, 10$ and 50 obtained by the cyclic torsion test, are shown in Fig. 7.

As can be seen in Fig. 7a, torque M increases in proportion to the angle of twist per unit length θ at temperature $T = \text{RT}$. Although large residual angle of twist appears after unloading, the residual deformation disappears by heating under no-load, giving evidence of the SME.

As can be seen in Fig. 7b, the rate of increase in torque $dM/d\theta$ increases gradually with an increase in angle of twist per unit length θ at $T = 358 \text{ K}$. In the case of high temperature, the rate of increase in deformation resistance increases with an increase in θ . Angle of twist recovers during unloading, showing SE.

Comparing the torsion deformation properties of the SMA thin strip at the number of cycles $N = 1, 10$ and 50 , variation in the properties by repetition is slight in both $T = \text{RT}$ and 358 K . The reason why the properties vary slightly with cycling is the fact that the MT occurs only at the edge element in the specimen as observed in Fig. 6 and elastic deformation occurs in the internal element, resulting in slight variation in the cyclic deformation properties.

In the previous paper [11], it was shown that the relation between torque M and angle of twist per unit length θ in the loading process is expressed by the following equation:

$$(3.1) \quad M = awt^3G\theta(T - M_s)$$

at temperatures T above A_s and M is constant at $T \leq A_s$, where G , w and t denote the modulus of rigidity, width and thickness, and coefficient a depends

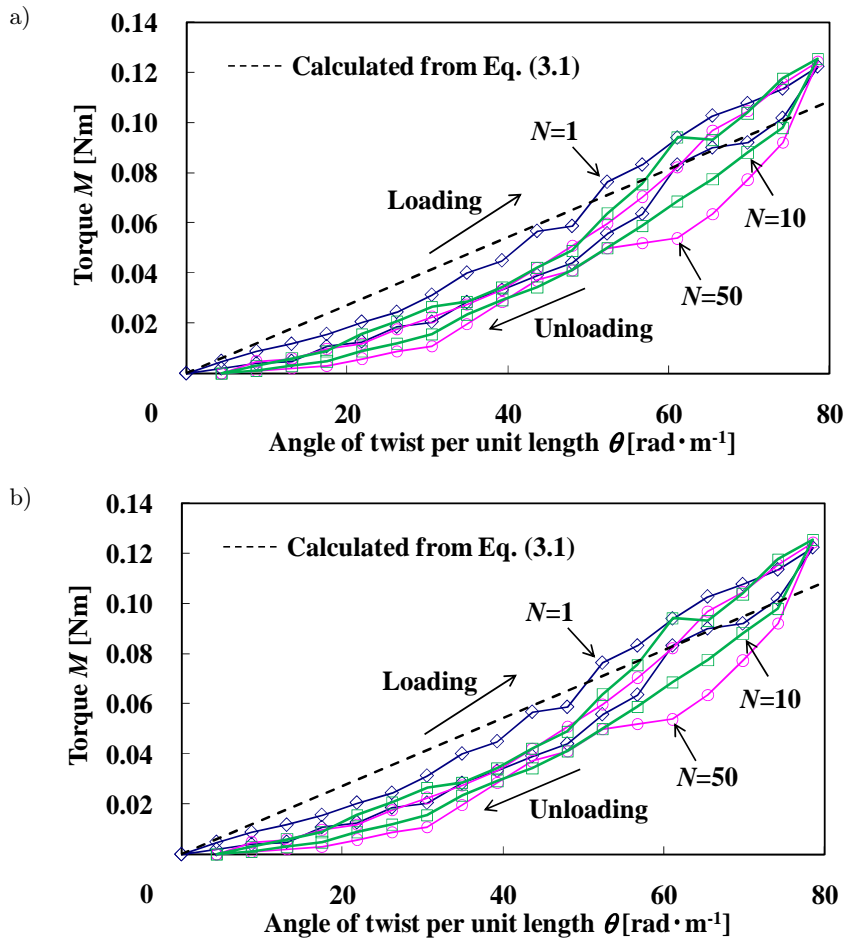


FIG. 7. Relationship between torque and angle of twist under cyclic torsion: a) $T = RT$,
b) $T = 358$ K.

on the ratio of width to thickness w/t . In the case of $T = 358$ K $> A_s$, the result calculated by Eq. (3.1) using the values $a = 1.62 \times 10^{-2}$ K⁻¹ and $G = 20$ GPa which were used in the previous paper [11], is shown by the broken line in Fig. 7b. As can be seen from Fig. 7b, though the inclination of downward convexity can not be expressed precisely, the relation in the loading process can be roughly estimated. In the case of $T = RT < A_s = 319$ K, the result calculated by Eq. (3.1), taking $T = A_s$, is shown by the broken line in Fig. 7a. As can be seen from Fig. 7a, the relation in the loading process can be approximated well. As can be understood from the discussion of Fig. 7 mentioned above, Eq. (3.1) is useful for estimation of torque in the loading process in designing SMA-thin strip elements.

3.4. Torsion fatigue properties

The fatigue life curves on alternating fatigue and pulsating fatigue, expressed by the relations between the maximum angle of twist per unit length θ_{\max} and the number of cycles to failure N_f for SMA thin strip obtained from the torsion fatigue test are shown in Fig. 8, expressed in a logarithmic scale.

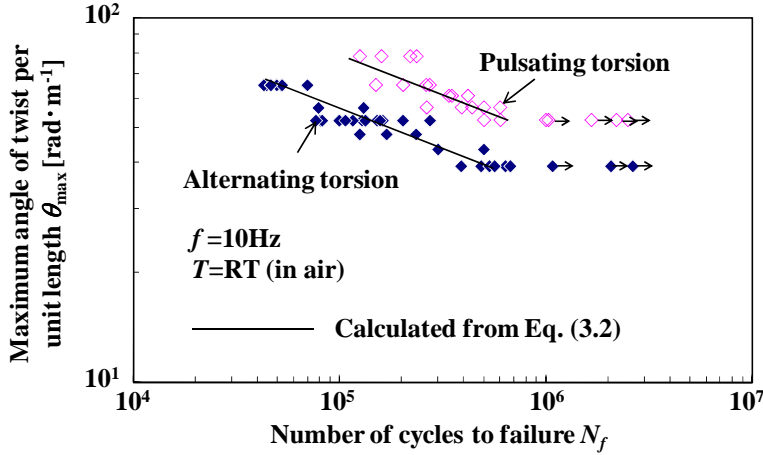


FIG. 8. Fatigue life curves of SMA thin strip for alternating torsion and pulsating torsion.

As can be seen in Fig. 8, the number of cycles to failure N_f decreases with an increase in the maximum angle of twist per unit length θ_{\max} in the region of low-cycle fatigue, where N_f changes depending on θ_{\max} . This relation is approximated by a straight line on the logarithmic graph. The fatigue life curve in the region of low-cycle fatigue seems therefore to be expressible by an equation similar to that already obtained for the fatigue life curve of TiNi SMA wires under bending [7, 8]. This can be seen in Eq. (3.2):

$$(3.2) \quad \theta_{\max} \cdot N_f^{\beta} = \alpha,$$

$$\begin{cases} \beta = 0.19, & \alpha = 500 \text{ rad} \cdot \text{m}^{-1} : \text{Alternating torsion,} \\ \beta = 0.22, & \alpha = 1000 \text{ rad} \cdot \text{m}^{-1} : \text{Pulsating torsion,} \end{cases}$$

where α and β represent θ_{\max} where $N_f = 1$ and the slope of the $\log \theta_{\max} - \log N_f$ curve, respectively. The calculated results obtained from Eq. (3.2) are shown by the solid lines in Fig. 8. As can be seen, the low-cycle fatigue life curves are well matched by the solid calculation lines.

Comparing the fatigue life of alternating torsion and pulsating torsion, the number of cycles to failure N_f for alternating torsion is smaller than that for pulsating torsion by 1/5 at the same maximum angle of twist per unit length θ_{\max} ,

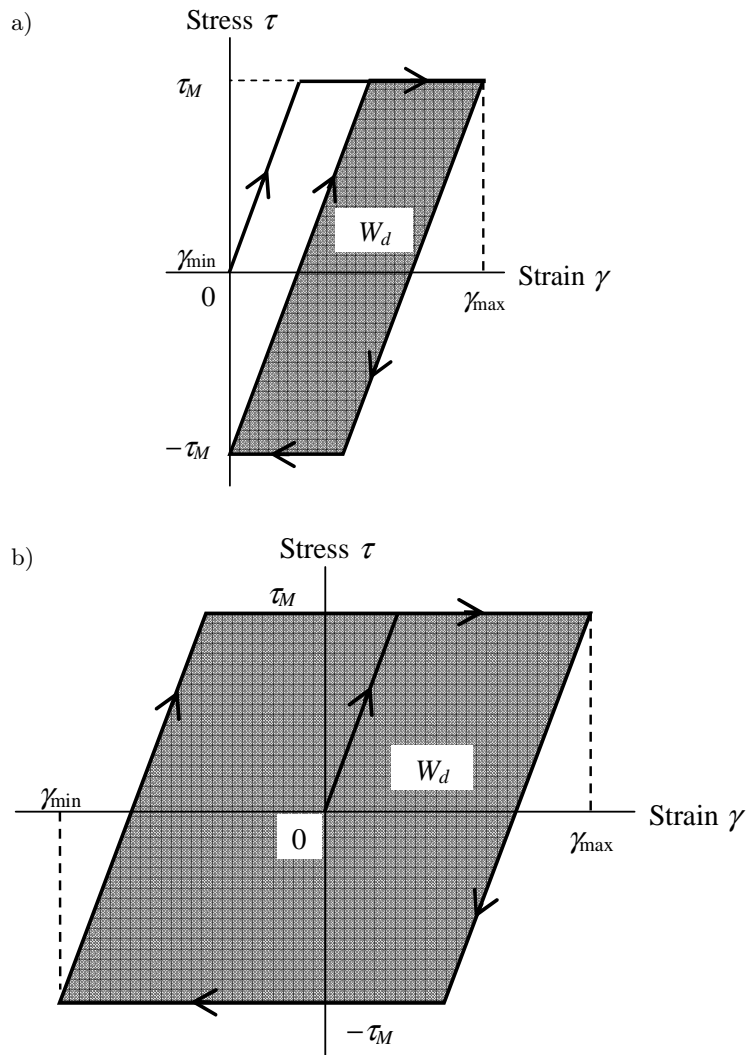


FIG. 9. Stress-strain diagram of surface element in torsion showing dissipated work W_d in each cycle: a) pulsating torsion, b) alternating torsion.

and therefore the fatigue life is shorter by $1/5$. The relations between torsional stress τ and torsional strain γ subjected to pulsating torsion and alternating torsion are schematically shown in Fig. 9. In Fig. 9, it is assumed that the MT stress τ_M in clockwise torsion is equal to that in counterclockwise torsion. Although the material is subjected to the maximum torsion deformation once in each cycle in the case of pulsating torsion, it is subjected to both the maximum torsion deformation and the minimum torsion deformation of the same absolute value in the case of alternating torsion. That is, in the case of alternating fatigue,

the material is subjected to the positive and negative maximum torsion deformation in each cycle. Therefore, the dissipated work W_d in each cycle, which is prescribed by the area surrounded by the hysteresis loop in Fig. 9, is larger in the case of alternating torsion. As a result, fatigue damage in alternating torsion is large, resulting in a short fatigue life. If the influence of W_d on N_f is evaluated based on tensile strain ε of the edge of the thin strip which causes the fatigue crack initiation, it can be explained as follows. As can be seen in Fig. 5, the tensile strain ε which corresponds to $\theta_{\max} = 50 \sim 70 \text{ rad} \cdot \text{m}^{-1}$ in the fatigue failure region is about 0.75%. Taking elastic modulus $E = 45 \text{ GPa}$, the MT stress $\sigma_M = 100 \text{ MPa}$, maximum tensile strain $\varepsilon_{\max} = 0.75\%$ from the stress-strain curve at RT shown in Fig. 3, W_d is obtained from the similar parallelogram as shown in Fig. 9. The obtained value of W_d is $0.6 \text{ MJ} \cdot \text{m}^{-3}$ for pulsating torsion and $2.6 \text{ MJ} \cdot \text{m}^{-3}$ for alternating torsion. Therefore, W_d in alternating torsion is larger than that in pulsating torsion by 4.3 times. The difference of W_d affects the fatigue damage, and the fatigue life becomes about 1/5 in alternating torsion.

The maximum angle of twist per unit length θ_{\max} for the fatigue limit at which the fatigue life curve becomes horizontal is $35 \text{ rad} \cdot \text{m}^{-1}$ for alternating torsion and $50 \text{ rad} \cdot \text{m}^{-1}$ for pulsating torsion, respectively. Since the MT starting angle of twist per unit length is about $30 \text{ rad} \cdot \text{m}^{-1}$, the maximum angle of twist per unit length at the fatigue limit in alternating torsion exists in the vicinity of the MT starting point.

3.5. Two-way opening and closing door model

Photographs of the rotary movement of an opening and closing door model using an SMA thin strip (SME-SMA strip) which shows the SME and an SMA thin strip (SE-SMA strip) which shows SE at RT under heating and cooling, are shown in Fig. 10. The SME-SMA thin strip is the same as the specimen used in the present study. The SE-SMA strip with a thickness of $t = 0.25 \text{ mm}$ and a width of $w = 2.5 \text{ mm}$ was a TiNi-SMA thin strip which was heat-treated to memorize a flat plane. In the initial state at RT, the SE-SMA strip was mounted to be in a flat plane and the SME-SMA strip was mounted at the total angle of twist $\phi = \pi/2$. The SME-SMA strip was heated by Joule heat through electric current. As can be seen in Fig. 10, the door is closed in the initial state, since torque of SE-SMA strip M_{SE} is larger than that of the SME-SMA strip M_{SME} . Since recovery torque appears by heating the SME-SMA strip and the relation of the torque changes into $M_{\text{SME}} < M_{\text{SE}}$, the SME-SMA strip recovers a flat plane and therefore the door is opened. When the SME-SMA strip is cooled thereafter, the relation of torque varies again into $M_{\text{SME}} > M_{\text{SE}}$. Therefore, the SE-SMA strip recovers a flat plane, resulting in closing the door.

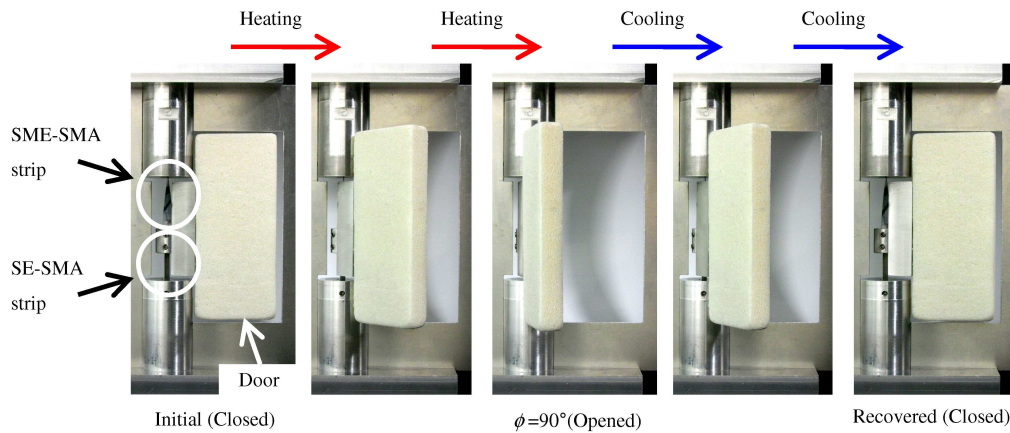


FIG. 10. Photographs of two-way rotary movement of a door driven by SMA thin strips during heating and cooling.

Thus, if two kinds of SMA thin strips which show the SME and SE are used, a two-way rotary driving element with a small and simple mechanism can be developed.

4. Conclusions

In order to develop the rotary driving element with SMA thin strip, the torsional deformation property, cyclic deformation property and fatigue property of a TiNi SMA thin strip were investigated. The results obtained can be summarized as follows.

1. In the SMA thin strip subjected to torsion, the MT appears along the edge of the strip due to elongation of the edge of the strip and grows to the central part. The rate of increase in elongation of the edge of the strip increases gradually with an increase in angle of twist.

2. Torque increases in proportion to the angle of twist. The torsion deformation properties vary slightly with cycling.

3. The number of cycles to failure decreases with an increase in the maximum angle of twist in torsion fatigue. The fatigue life in pulsating torsion is longer than that in alternating torsion by five times at the same maximum angle of twist in the region of low-cycle fatigue. The maximum angle of twist per unit length at the fatigue limit in alternating torsion is $35 \text{ rad} \cdot \text{m}^{-1}$ which is close to the MT starting point of about $30 \text{ rad} \cdot \text{m}^{-1}$.

4. Based on the two-way rotary movement of an opening and closing door model by using two kinds of SMA thin strip which show the SME and SE, it is confirmed that a rotary driving element with a small and simple mechanism can be developed by using the SMA thin strip.

Acknowledgments

This study was performed as the bilateral joint research project between Aichi Institute of Technology and Institute of Fundamental Technological Research supported by the Japan Society for Promotion of Science and the Polish Academy of Sciences. The experimental work for this study was carried out with the assistance of students in Aichi Institute of Technology, to whom the authors wish to express their gratitude. The authors also wish to extend thanks to the administrators of Scientific Research (C) in Grant-in-Aid for Scientific Research by the Japan Society for Promotion of Science for financial support.

References

1. H. FUNAKUBO [Ed.], *Shape Memory Alloys*, Gordon and Breach Science Pub., 1–60, 1987.
2. T.W. DUERIG, K.N. MELTON, D. STOCKEL, C.M. WAYMAN [Eds.], *Engineering Aspects of Shape Memory Alloy*, Butterworth-Heinemann, 1–35, 1990.
3. K. OTSUKA, C.M. WAYMAN [Eds.], *Shape Memory Materials*, Cambridge University Press, 1–49, 1998.
4. T. SABURI [Ed.], *Shape Memory Materials*, Trans Tech Pub., 315–366, 2000.
5. Y.Y. CHU, L.C. ZHAO [Eds.], *Shape Memory Materials and Its Applications*, Trans Tech Pub., 177–284, 2002.
6. R.L. HOLTZ, K. SADANANDA, M.A. IMAM, *Fatigue Thresholds of TiNi Alloy Near the Shape Memory Transition Temperature*, Int. J. Fatigue, **21**, 137–145, 1999.
7. R. MATSUI, H. TOBUSHI, Y. FURUICHI, H. HORIKAWA, *Tensile Deformation and Rotating-Bending Fatigue Properties of a Highelastic Thin Wire, a Superelastic Thin Wire, and a Superelastic Thin Tube of NiTi Alloys*, Trans. ASME, J. Eng. Mater. Tech., **126**, 384–391, 2004.
8. R. MATSUI, S. MAKINO, H. TOBUSHI, Y. FURUICHI, F. YOSHIDA, *Influence of Strain Ratio on Bending Fatigue Life and Fatigue Crack Growth in TiNi Shape-Memory Alloy Thin Wires*, Mater. Trans., **47**-3, 759–765, 2006.
9. J.H. MABE, R.T. RUGGERI, E. ROSENZWEIG, C.J. YU, *NiTinol Performance Characterization and Rotary Actuator Design*, Smart Struct. Mater: 2004, Proc. SPIE, **5388**, 95–109, 2004.
10. J.H. MABE, F.T. CALKINS, R.T. RUGGERI, *Full-scale Flight Tests of Aircraft Morphing Structures using SMA Actuators*, Proc. of SPIE, **6525**-65251C, 1–12, 2007.
11. H. TOBUSHI, T. SAKURAGI, Y. SUGIMOTO, *Deformation and Rotary Driving Characteristics of a Shape-Memory Alloy Thin Strip Element*, Mater. Trans., **49** 1, 151–157, 2008.
12. L.C. BRINSON, I. SCHMIDT, R. LAMMERING, *Stress-Induced Transformation Behavior of a Polycrystalline NiTi Shape Memory Alloy: Micro and Macromechanical Investigations via In Situ Optical Microscopy*, J. Mech. Phys. Solids, **52**, 1549–1571, 2004.
13. D. FAVIER, H. LOUCHE, P. SCHLOSSER, L. ORGEAS, P. VACHER, L. DEBOVE, *Homogeneous and Heterogeneous Deformation Mechanisms in an Austenitic Polycrystalline*

- Ti-50.8at%Ni Thin Tube under Tension. Investigation via Temperature and Strain Fields Measurements*, Acta Materialia, **55**, 16, 5310–5322, 2007.
14. E.A. PIECZYSKA, H. TOBUSHI, S.P. GADAJ, W.K. NOWACKI, *Superelastic Deformation Behaviors Based on Phase Transformation Bands in TiNi Shape Memory Alloy*, Mater. Trans., **47**, 3, 670–676, 2006.
 15. K. HASHIMOTO, M. TOKUDA, T. INABA, A. SHIODE, P. SITTNER, B. BUNDARA, *Experimental Research on Deformation of Ti-Ni SMA under Complex Loading Conditions*, Key Engineering Materials, **233–236**, 547–552, 2003.
 16. S.T. TIMOSHENKO, J.N. GOODIER, *Theory of Elasticity*, 3rd ed., McGraw-Hill, 307–313, 1982.

Received October 15, 2008; revised version March 6, 2009.
